Supplementary Information

for

Probing Ag nanoparticle surface oxidation in contact with (in)organics: An x-ray scattering and fluorescence yield approach

Clement Levard[1,2]*, *F. Marc Michel*[1,3], *Yingge Wang*[1], *Yongseong Choi*[4], *Peter Eng*[4], *Gordon E. Brown Jr.*[1,2,3]

[1] Surface and Aqueous Geochemistry Group, Department of Geological & Environmental Sciences, Stanford University, Stanford, CA 94305, USA

[2] Center for Environmental Implications of NanoTechnology (CEINT), P.O. Box 90287, Duke University, Durham, NC 27708-0287, USA.

[3] Stanford Synchrotron Radiation Lightsource, SLAC National Accelerator Laboratory, 2575 Sand Hill Road, Menlo Park, CA 94025, USA

[4] Consortium for Advanced Radiation Sources, University of Chicago, Chicago, IL 60637, USA

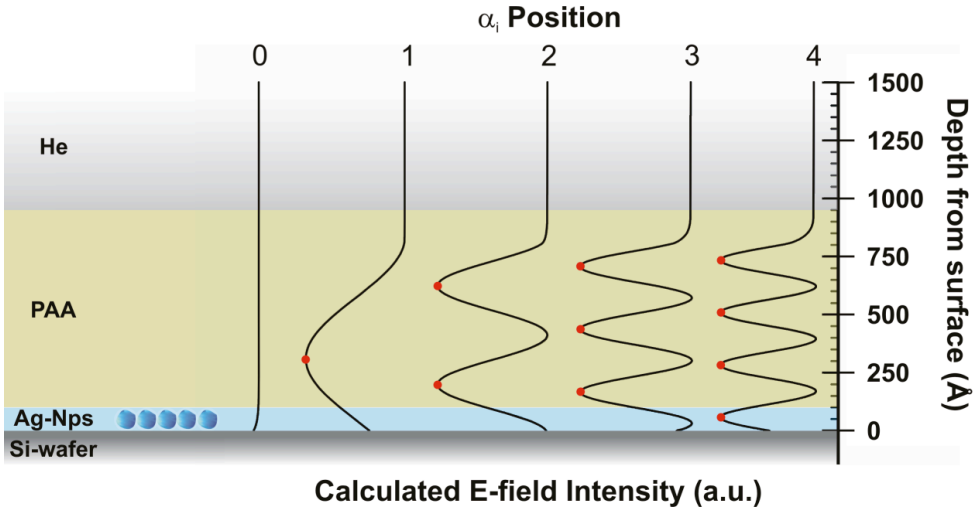

Figure S1 | Calculated electric field (E-field) intensity at selected incidence angles. Below the critical angle for total external reflection the interference of incoming and outgoing grazing-incidence x-rays results in a periodic E-field intensity variation known as the long period XSW (Bedzyk et al, 1990). At low incidence angles (e.g., α_i position 0, also shown in Figure 4b) a standing wave node is at the reflecting (Si-wafer) surface and the first antinode is at infinity. As the angle of incidence increases the first antinode (α_i position 1) moves toward the surface and provides sensitivity to the distribution of elements (XSW-FY) and phases (XSW-XRD) in the PAA film. As the angle of incidence is increased further, the second, third, and higher-order antinodes also move toward the surface (α_i positions 2 and 3) and eventually an antinode is located in the PVP-coated Ag-Nps layer (α_i position 4). As such, in this study FY and XRD data collected at low incidence angles are more sensitive to the PAA film while higher angles are sensitive to the Ag-Nps layer.

Bedzyk, M. J., Bommarito, G. M., Caffrey, M. & Penner, T. L. Diffuse-Double Layer at a Membrane-Aqueous Interface Measured with X-ray Standing Waves. *Science* **248**, 52-56 (1990).

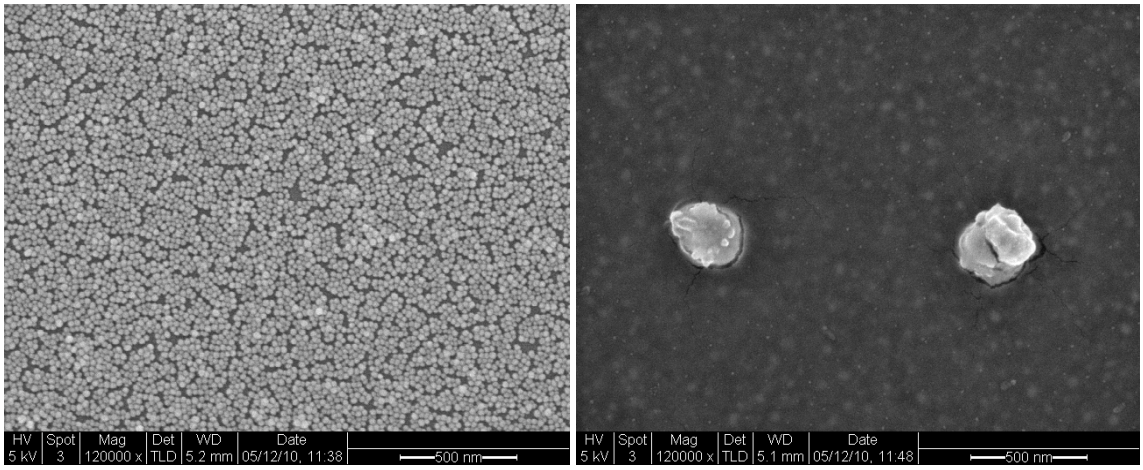

Figure S2 | SEM imaging of the PVP-coated Ag-Nps film before (left) and after (right) reaction with the PAA solution. Large particles or aggregates approximately 200 nm in diameter are observed after the reaction with the PAA solution.

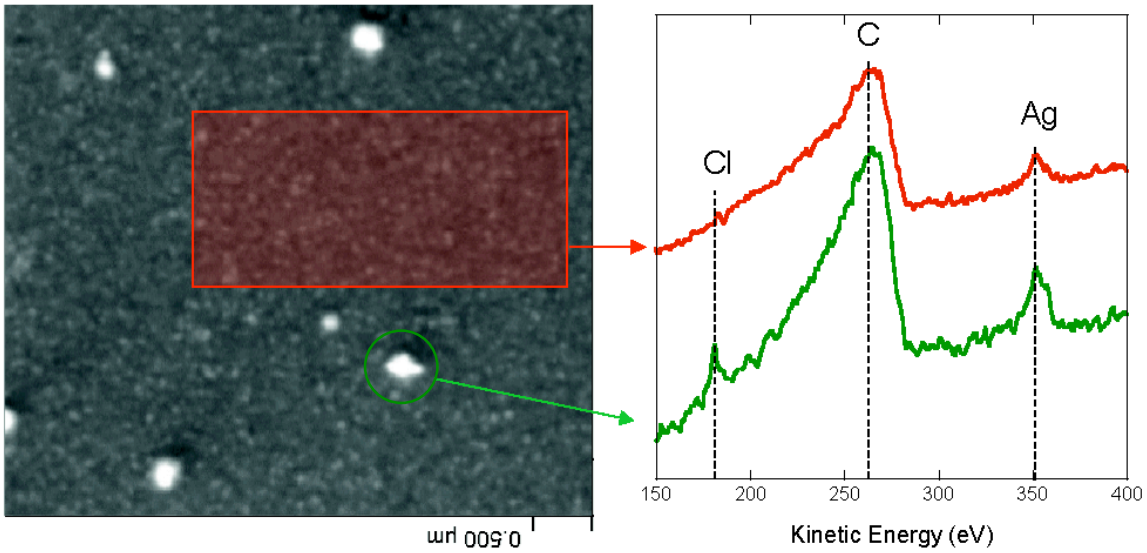

Figure S3 | Auger analysis of the particles/aggregates observed after reaction with PAA. Two areas were analyzed, one corresponding to the background (red area) and a second centered on the larger particle/aggregates protruding from the PAA film (green area). Two main elements were detected in the background: C (from PAA) and Ag. Analysis of the green area shows the presence of Cl in addition to Ag and C. This observation coupled with the results of XRD analysis strongly suggests that these particles correspond to $AgCl_{(s)}$ in the PAA film.

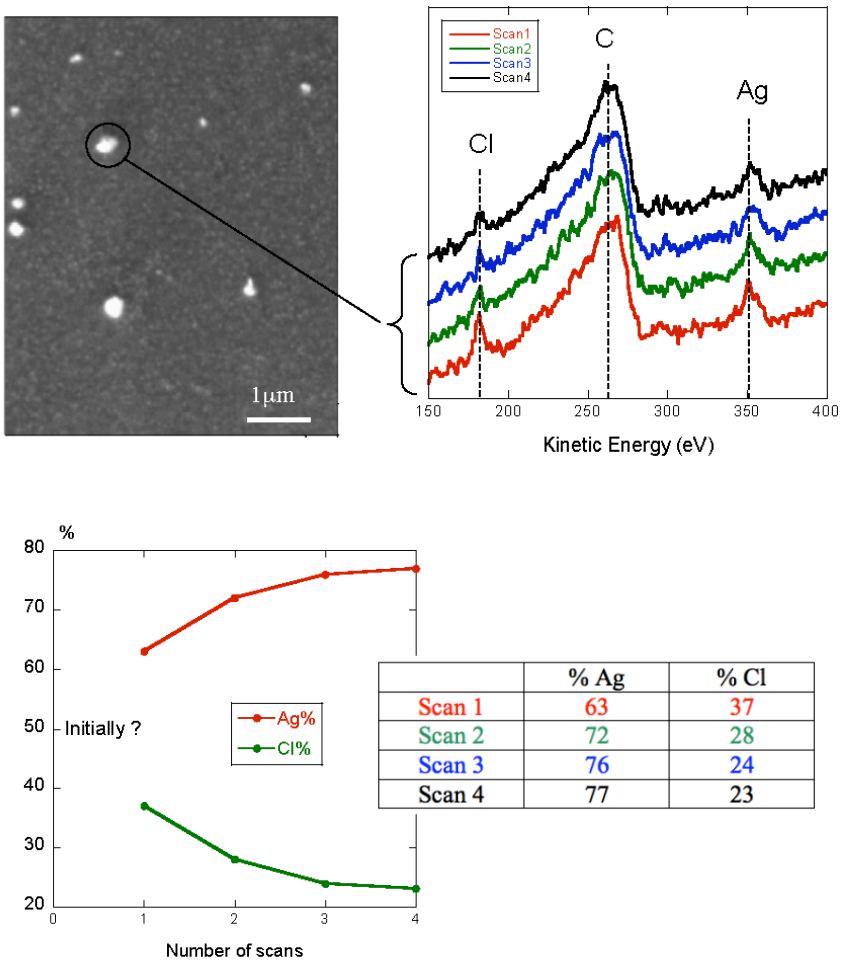

	% Ag	% Cl
Scan 1	63	37
Scan 2	72	28
Scan 3	76	24
Scan 4	77	23

Figure S4 | Quantitative analysis of the Auger spectra for Ag and Cl. Ag:Cl ratios ranging from 1.7 to 3.4 were measured during repeated scans for a particle/aggregate in the PAA film (Table). These ratios are significantly higher than what is expected based on the stoichiometry of AgCl (Ag/Cl = 1). A systematic decay in Auger intensity (top right) with increasing electron fluence on the same particle (top left, beam characteristics: 5 kV, 3 nA). Such changes are consistent with electron beam-stimulated desorption of Cl. The initial values of Ag and Cl estimated by extrapolation to zero electron fluence (bottom) correspond to ~50% Ag and ~50% Cl and are generally consistent with the stoichiometry of AgCl.

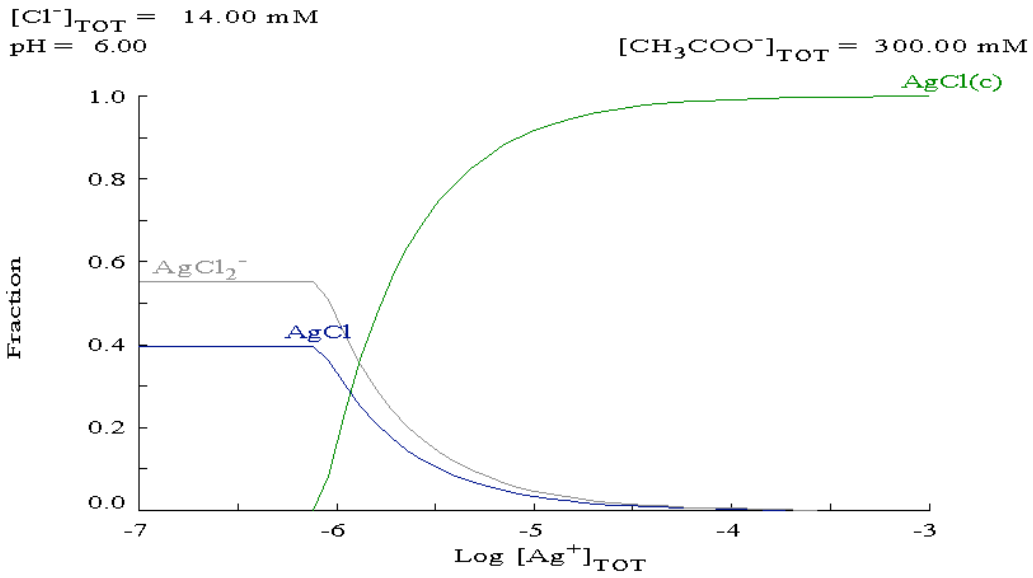

Figure S5 | Thermodynamic simulation of the speciation of Ag. The speciation of silver was calculated considering the initial concentration of carboxyl (0.3 mol.L^{-1}) and Cl (0.014 mol.L^{-1}) initially present in the PAA solution. The concentration of Ag-Nps in our system is 0.001 mol.L^{-1}. This simulation suggests that Ag^+ has a higher affinity for Cl^- than for the carboxyl despite the high CH_3COO^-:Cl^- ratio (21.4).